

Thermal expansion and electrochemical properties of $\text{La}_{0.7}\text{AE}_{0.3}\text{CuO}_{3-\delta}$ ($\text{AE}=\text{Ca, Sr, Ba}$) cathode materials for IT-SOFCs

Xifeng Ding · Ling Gao · Yingjia Liu · Yifeng Zhen ·
Lucun Guo

Received: 29 December 2006 / Accepted: 9 May 2007 / Published online: 1 June 2007
© Springer Science + Business Media, LLC 2007

Abstract Alkaline earth metals (Ca, Sr, Ba) substituted lanthanum copper oxides were investigated to evaluate their potentials as cathode materials for intermediate temperature solid oxide fuel cell (IT-SOFC). The crystal structure, thermal expansion and electrochemical performance of $\text{La}_{1-x}\text{AE}_x\text{CuO}_{3-\delta}$ ($x=0.3$, AE=Ca, Sr, Ba) were studied by X-ray diffraction, thermal dilatometer and impedance spectra, respectively. By lowering the size of the A-site cation in ABO_3 perovskite, a lower thermal expansion and polarization resistance were obtained for Ca-doped $\text{LaCuO}_{3-\delta}$ cathode which showed an area specific resistance of $0.19 \Omega \text{ cm}^{-2}$ under open circuit potential conditions at 800°C , and a polarization overpotential of 52 mV at a current density of 0.1 A/cm^2 at 700°C , being a potential candidate of cathode material for IT-SOFCs.

Keywords SOFC · Cathode · Thermal expansion · Electrochemical performance

1 Introduction

Mixed electronic and ionic conducting perovskite oxides, exhibiting high electrical and oxide ionic conductivity [1–3], and excellent cathode activity [4, 5], are of great practical

significance in various electrochemical applications such as oxygen electrode materials for solid oxide fuel cells (SOFCs) [6–9], catalysis and oxygen separation membranes [10]. Among them, mixed conducting lanthanum copper oxides ($\text{LaCuO}_{3-\delta}$) are of special interest as potential cathode material for intermediate temperature solid oxide fuel cells (IT-SOFCs) recently [11–14]. Copper oxide possesses superior electrical conductivity and high activity for the reduction of oxygen to manganite-based cathodes in the intermediate temperature range of 500 – 800°C . However, copper oxide cathodes exhibited high thermal expansion coefficients (TECs) ($\sim 17 \times 10^{-6} \text{ K}^{-1}$ [11]) that are unmatched to the doped ceria electrolyte ($\sim 12 \times 10^{-6} \text{ K}^{-1}$ [15]).

Some element substitutions in A and /or B sites in ABO_3 perovskite-type of $\text{La}_{1-x}\text{Sr}_x\text{CuO}_{3-\delta}$ have been attempted in order to synthesize more favorable cathode materials [16–18]. More work has been done with regard to the substitution at B-site, for instance, $\text{La}_{1-x}\text{Sr}_x\text{Cu}_{1-y}\text{Fe}_y\text{O}_{3-\delta}$ with $x=0.3$ and $y=0.8$ showed a peak conductivity above 250 S cm^{-1} at temperatures less than 650°C [16]. However, relatively few results have been reported dealing with the substitution at A-site [Y22]. The Sr-doped $\text{LaCuO}_{3-\delta}$ based cathode materials have been recently investigated by several researchers [11, 12, 14], and showed potential materials for IT-SOFCs. Since Ca and Ba are also belong to the same main group elements, it is expected that Ca-doped $\text{LaCuO}_{3-\delta}$ (LCC) and Ba-doped $\text{LaCuO}_{3-\delta}$ (LBC) should exhibit the similar or even better performance for being used as IT-SOFC cathodes.

In the present work, $\text{La}_{1-x}\text{AE}_x\text{CuO}_{3-\delta}$ (AE=Ca, Sr, Ba, $x=0.3$) was investigated on crystal structure and TEC compatibility towards $\text{Sm}_{0.2}\text{Ce}_{0.8}\text{O}_{2-\delta}$ electrolyte. In addition, the electrochemical performance was determined by impedance spectroscopy between 500°C and 800°C .

X. Ding (✉) · L. Gao · Y. Liu · Y. Zhen · L. Guo
College of Materials Science and Engineering,
Nanjing University of Technology,
Nanjing, Jiangsu 210009, People's Republic of China
e-mail: dingxifeng2002@163.com

L. Guo
e-mail: lc-guo@163.com

2 Experimental

2.1 Powder synthesis

$\text{La}_{0.7}\text{AE}_{0.3}\text{CuO}_{3-\delta}$ and $\text{Sm}_{0.2}\text{Ce}_{0.8}\text{O}_{2-\delta}$ powders were prepared by the conventional solid state reaction method using La_2O_3 (99.99%), SrCO_3 (99%), CaCO_3 (99%), BaCO_3 (99%), CuO (98%), CeO_2 (99%), Sm_2O_3 (99.99%) as starting materials. The raw materials were weighted according to stoichiometric ratio and mixed for 8 h in distilled water with zirconia grinding media. The $\text{La}_{0.7}(\text{AE})_{0.3}\text{CuO}_{3-\delta}$ and $\text{Sm}_{0.2}\text{Ce}_{0.8}\text{O}_{2-\delta}$ powders were obtained after being calcined in air at 800°C and at 1200°C for 2 h, respectively.

2.2 Cell preparation

Symmetrical electrochemical cells consisting of porous $\text{La}_{0.7}(\text{AE})_{0.3}\text{CuO}_{3-\delta}$ electrode and dense SDC electrolyte were fabricated. Uniaxially pressed SDC electrolytes disks were sintered at 1560°C for 2 h in air. After sintering, the diameter of the pellets was about 15 mm and the thickness was about 1 mm. The ink for electrode deposition was prepared by mixing the as-prepared powder with ethyl cellulose and terpinol in appropriate ratio. Then, $\text{La}_{0.7}(\text{AE})_{0.3}\text{CuO}_{3-\delta}$ pastes with an effective electrode area of 1 cm^2 were printed twice on each side of the SDC disks and then calcined at 950°C for 2 h in air. The thickness of the $\text{La}_{0.7}(\text{AE})_{0.3}\text{CuO}_{3-\delta}$ cathodes is about 20 μm after calcination. Current collector using silver paste was then coated onto the surfaces of $\text{La}_{0.7}(\text{AE})_{0.3}\text{CuO}_{3-\delta}$ electrodes and sintered at 600°C for 30 min. And Pt grids and leads were stuck with Ag current collector for the electrochemical properties measurements.

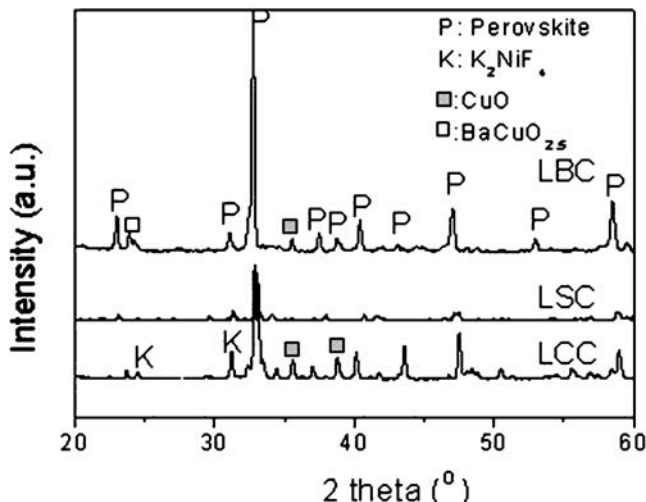


Fig. 1 X-ray diffraction patterns of $\text{La}_{0.7}\text{AE}_{0.3}\text{CuO}_{3-\delta}$ (AE=Ca, Sr, Ba) fired at 1223 K for 2 h in air

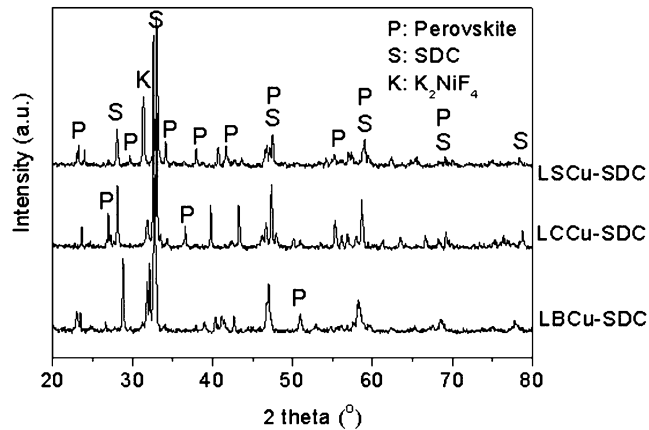


Fig. 2 X-ray Diffraction patterns of mixture powders of $\text{La}_{0.7}\text{AE}_{0.3}\text{CuO}_{3-\delta}$ (AE=Sr, Ca, Ba) with SDC electrolyte (LSC-SDC, LCC-SDC, LBC-SDC) fired at 1273 K for 2 h

2.3 Characterization

$\text{La}_{0.7}\text{AE}_{0.3}\text{CuO}_{3-\delta}$ powders were determined for phase purity via X-ray diffraction (XRD, D/max-III, Rigaku) with $\text{CuK}\alpha$ radiation in the 2θ range from 18° to 60°. The thermal expansion of the rectangular $\text{La}_{0.7}\text{AE}_{0.3}\text{CuO}_{3-\delta}$ specimens (sintered at 1000°C for 2 h) were measured from room temperature to 800°C in air, using a dilatometer (RPZ-01, Luoyang, China), with a heating rate of 5°C/min. AC impedance spectroscopy measurements of the electrode materials on SDC electrolyte were carried out with excitation potentials of 10 mV over a frequency range from 1 MHz to 0.1 Hz generated by an impedance analyzer (1260A Impedance analyzer, Solartron, UK) and an electrochemical interface (1287A Potentiostat, Solartron, UK) in the temperature range from 500 to 800°C. Cathodic polarization tests of the electrode materials on SDC electrolyte were tested on the half cells with Ag paste as counter electrode and reference electrode within 500–800°C in air. The applied voltages to the cathodes were changed from 0 to 0.4 V. The overpotential (η) of the cathodes under cathodic polarization was estimated by the following equation:

$$\eta = E - IR_s \quad (1)$$

where E , I , and R_s indicate the applied cathodic voltage, current and ohmic resistance measured by the impedance spectra, respectively. The definition and derivation of R_s values will be described in the next section.

3 Results and discussion

3.1 Phase composition

The XRD patterns of $\text{La}_{0.7}\text{AE}_{0.3}\text{CuO}_{3-\delta}$ (AE=Ca, Sr, Ba) samples are exhibited in Fig. 1. The results exhibited that

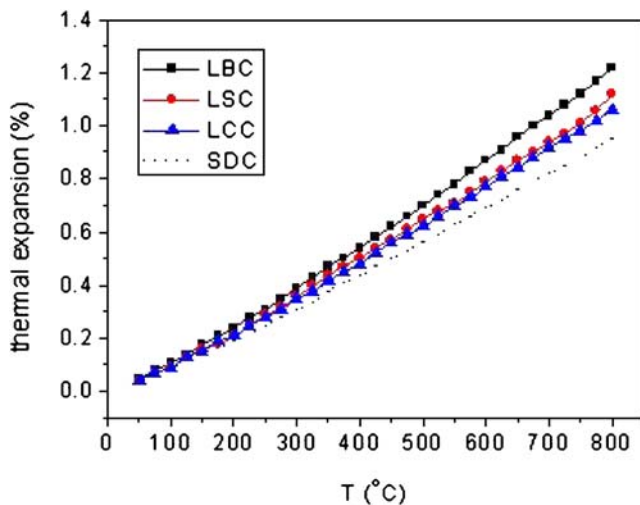


Fig. 3 Thermal expansion of $\text{La}_{0.7}\text{AE}_{0.3}\text{CuO}_{3-\delta}$ ($\text{AE}=\text{Ca}, \text{Sr}, \text{Ba}$) from 50 to 800°C in air

the $\text{La}_{0.7}\text{Sr}_{0.3}\text{CuO}_{3-\delta}$ sample was single-phase ABO_3 -type perovskite solid solutions without any detectable impurity phases, which is consistent with the results of Yu et al. [11]. However, the pattern of $\text{La}_{0.7}\text{Ca}_{0.3}\text{CuO}_{3-\delta}$ power contains the reflections of A_2BO_4 perovskite-related compound and CuO as second phases, in addition to those of perovskite phase. The K_2NiF_4 -type perovskite related phase could be attributed to the instability of perovskite phase at high temperatures [19]. And $\text{La}_{0.7}\text{Ba}_{0.3}\text{CuO}_{3-\delta}$ power contains a small amount of CuO and $\text{BaCuO}_{2.5}$ phases which may be due to the inhomogeneity of mixed powders during the ball milling and the subsequent calcination.

When the IT-SOFC with $\text{La}(\text{AE})\text{CuO}_{3-\delta}$ as cathode materials operated at 800°C, the local high-temperature areas on the $\text{La}(\text{AE})\text{CuO}_{3-\delta}/\text{SDC}$ interface may be higher than 800°C, which may cause material problems including thermal stress at the electrolyte/electrode interface, interdiffusion between cell components, and chemical reaction between electrode and electrolyte material. These material damages may degrade the performance of SOFCs. Thus, the chemical compatibility between $\text{La}(\text{AE})\text{CuO}_{3-\delta}$ and SDC is necessary to further investigate. The reactivity of $\text{La}_{0.7}\text{AE}_{0.3}\text{CuO}_{3-\delta}$ with SDC was carried out at 1273 K for 2 h. The typical XRD patterns of the mixtures are shown in

Table 1 TECs ($\times 10^{-6} \text{ K}^{-1}$) of $\text{La}_{0.7}\text{Sr}_{0.3}\text{CuO}_{3-\delta}$ ($\text{AE}=\text{Ca}, \text{Sr}, \text{Ba}$) and SDC in air.

Composition	TEC ($\times 10^{-1} \text{ °C}^{-1}$)	
	20–600°C	20–800°C
SDC	11.9	12.2
$\text{La}_{0.7}\text{Sr}_{0.3}\text{CuO}_{3-\delta}$	13.3	13.6
$\text{La}_{0.7}\text{Sr}_{0.3}\text{CuO}_{3-\delta}$	13.5	14.3
$\text{La}_{0.7}\text{Sr}_{0.3}\text{CuO}_{3-\delta}$	14.8	15.5

Fig. 2. It can be found that $\text{La}_{0.7}\text{AE}_{0.3}\text{CuO}_{3-\delta}$ yielded no reaction products and showed highly chemical compatibility with SDC electrolyte in the preparing and working conditions. Therefore, the performance of SOFC would not significantly degrade by the reaction between electrode and electrolyte for $\text{La}_{0.7}\text{AE}_{0.3}\text{CuO}_{3-\delta}/\text{SDC}$ system.

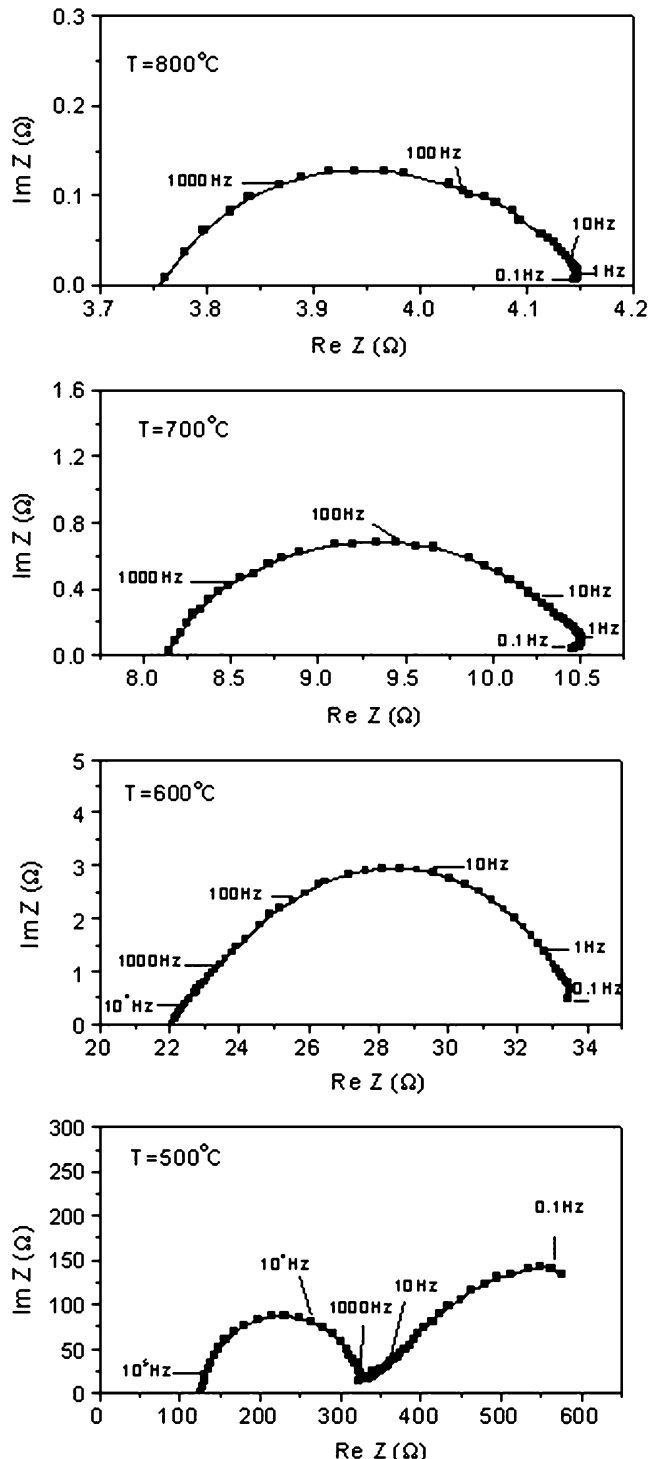


Fig. 4 Impedance spectra taken from $\text{La}_{0.7}\text{Ba}_{0.3}\text{CuO}_{3-\delta}$ (LBC) in air at various temperatures

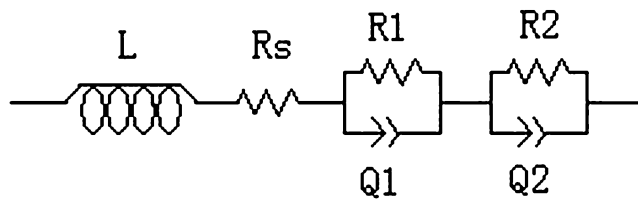


Fig. 5 Equivalent circuit of the electrode reaction

3.2 Thermal expansion

The thermal expansion behaviors of the $\text{La}_{0.7}\text{AE}_{0.3}\text{CuO}_{3-\delta}$ samples measured in the range of 200–800°C in air are exhibited in Fig. 3. The thermal expansion curve of SDC is also shown as dotted line for comparison. The $\text{La}_{0.7}\text{AE}_{0.3}\text{CuO}_{3-\delta}$ samples all show nearly straight line thermal expansion behavior whereas the slope increases at high temperatures, indicating the loss of lattice oxygen and the formation of oxygen vacancies [20]. The average TECs of the $\text{La}_{0.7}\text{AE}_{0.3}\text{CuO}_{3-\delta}$ measured in the range of 293–873 K and 293–1073 K in air are listed in Table 1. The TEC value increases from Ca to Ba with augment of ionic radii, which may be related to the ionic character of AE-O bond as discussed by Mori et al. [21] in the analogous lanthanum mangnates $\text{La}_{1-x}\text{AE}_{0.3-x}\text{MnO}_{3-\delta}$ (AE=alkaline-earth). The decreasing TEC from AE=Ba to Ca could be attributed to the decreasing ionic character of AE-O bond. The TEC compatibility between the cathode and electrolyte is desirable to avoid the delamination and fracture at the electrode/electrolyte interface at high operating temperatures. The TEC of $\text{La}_{0.7}\text{Ca}_{0.3}\text{CuO}_{3-\delta}$ is $13.6 \times 10^{-6} \text{ K}^{-1}$ from 293 to 1073 K, which is quite close to that of SDC electrolyte. Thus from the consideration of the thermal expansion compatibility, $\text{La}_{0.7}\text{Ca}_{0.3}\text{CuO}_{3-\delta}$ seem to be more favorable than the others.

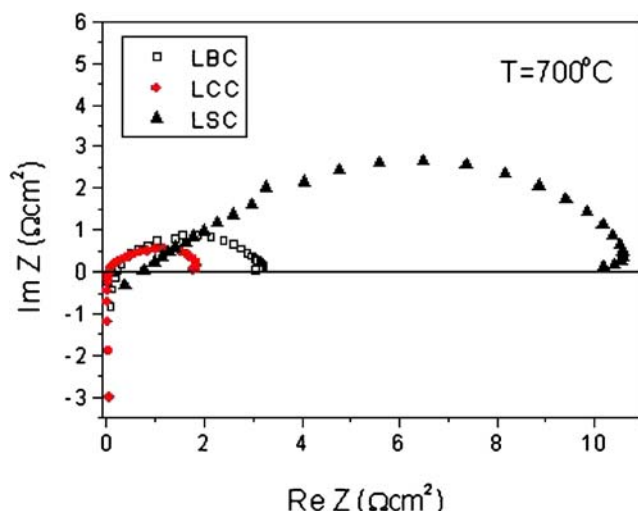


Fig. 6 Impedance spectra under open circuit conditions at 800°C for LBC, LCC and LSC cathodes fired at 950°C for 2 h

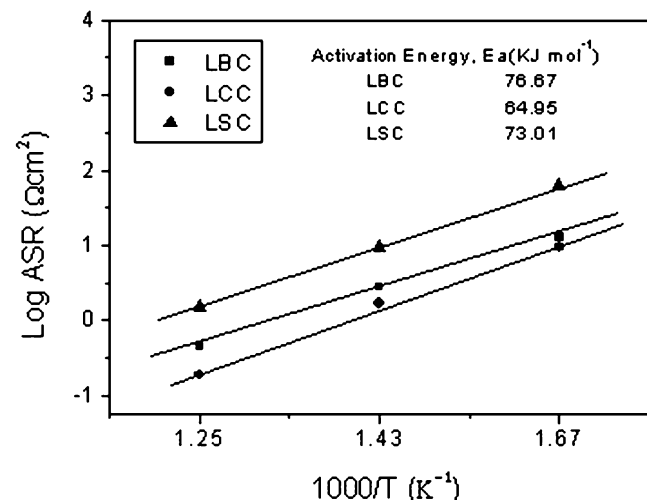


Fig. 7 Arrhenius plots of area-specific resistance of LBC, LCC and LSC in air from 600 to 800°C

3.3 Impedance spectroscopy

The evolution of impedance spectra for $\text{La}_{0.7}\text{Ba}_{0.3}\text{CuO}_{3-\delta}$ (LBC) with temperature is shown in Fig. 4. The shape of experimental impedance spectra is fairly similar to those previously reported in the literature [13]. The impedance spectra are evaluated by fitting impedance data with the equivalent circuit shown in Fig. 5, where R_s is the overall ohmic resistances including the electrolyte resistance, electrode resistance, lead resistance and contact resistance between the cell and Pt mesh. L is the inductance, which could be due to the Pt current/voltage probes or the high frequency phase. R_1 and R_2 are the electrode interface (polarization) resistance at high and low frequencies, Q_1 and Q_2 are the corresponding constant phase elements [22–24].

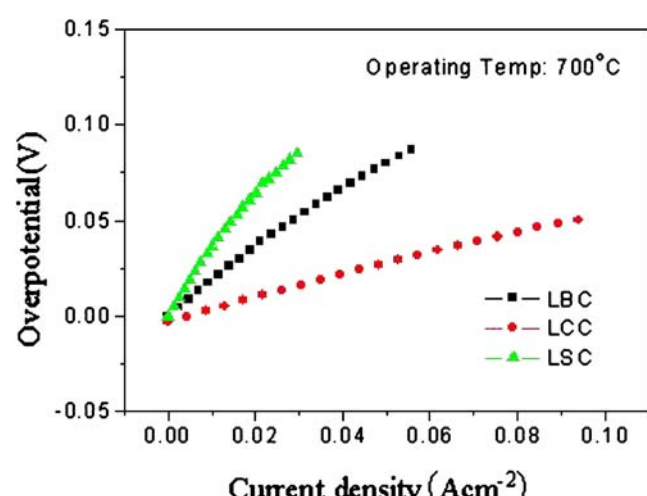


Fig. 8 Cathodic overpotential curves for $\text{La}_{0.7}(\text{AE})_{0.3}\text{CuO}_{3-\delta}$ (AE=Ba, Ca, Sr) in air at 700°C

According to the analysis of the AC impedance spectra, the spectra can be characterized by two arcs. The results indicate that there are at least two electrode processes occurred corresponding to the high and low frequency arcs during molecular oxygen reduction. At 500°C, the low and high frequency arc show an apparent separation. As the temperature increases, the two arcs are overlapped together, giving a single depressed arc.

Shown in Fig. 6 are area specific polarization resistances (ASRs) of $\text{La}_{0.7}\text{AE}_{0.3}\text{CuO}_{3-\delta}$ cathode measured at 700°C under open circuit condition. The ASRs are determined by the intersection of $\text{Re } Z$ axis of each impedance spectrum in the Nyquist plots. Here, the ohmic resistance of bulk electrolyte is subtracted in order to compare the catalytic activity of cathodes directly. It is apparent that LCC exhibits the lowest ASR. This is better shown in Fig. 7 for the cathodes compared at different temperatures in the form of Arrhenius plot, and the solid lines in Fig. 7 show the least-squares fitting of each set of data. From the slope of the fitting lines, the activation energies (E_a) the ASRs were calculated to be 65~77 kJ mol⁻¹ in the experimental conditions. The E_a values do not differ substantially for the three cathodes, indicating that the reaction mechanism is similar among these three different cathodes on SDC electrolyte. It is noted that the ASR values reported here for LCC cathode under open circuit conditions (1.68 Ω cm⁻² at 700°C and 0.19 Ω cm⁻² at 800°C) are even lower than the reported LSC cathode after passing 200 mA cm⁻² current (1.85 Ω cm⁻² at 700°C and 0.25 Ω cm⁻² at 800°C [11]). It is well known that the polarization resistance decreased with cathodic polarization voltage [25]. Thus, it is reasonable to expect that the electrochemical activity of LCC cathode could be further enhanced in the case of passing current.

3.4 Cathodic polarization

Figure 8 shows the effect of alkaline earth cations (Ca, Sr, Ba) on cathodic overpotential of $\text{La}_{0.7}\text{AE}_{0.3}\text{CuO}_{3-\delta}$ measured at 700°C. It can be seen that the cathodic overpotential was strongly affected by alkaline earth cations in the A site of copper-based perovskite oxide. Obviously, the cathodic overpotential decreased in the order of LCC<LBC<LSC, which is in agreement with the order of complex impedances (Figs. 6 and 7). Differences in electrochemical catalytic activity of the electrode materials can generally be attributed to the factors such as the electronic, ionic conductivity and microstructures [26]. The fact that the LCC cathode exhibits lower overpotential compared to LBC and LSC, implying a higher electrocatalytic activity which may be related to higher oxygen ionic conductivity and finer interfacial adhesion for its smallest TEC mismatch with SDC electrolyte (Table 1). The results are

in agreement with the previous report that Ca-doped PrMnO_3 had lower overpotential than Sr-doped PrMnO_3 [27]. The lowest polarization overpotential of 52 mV was measured for LCC at a current density of 0.1 A/cm². The electrochemical performance was also greatly influenced by the microstructures of the electrode/electrolyte interface [28]. Hence, it could be expected that the polarization performance would be further improved by optimizing the microstructures of the cathode.

4 Conclusions

The ABO_3 perovskite type oxides, $\text{La}_{0.7}\text{AE}_{0.3}\text{CuO}_{3-\delta}$ (AE=Ca, Sr, Ba), were investigated to evaluate their potential as cathode materials for IT-SOFCs. By lowering the size of the A-site cation, a lower thermal expansion and polarization resistance are obtained for Ca-doped $\text{LaCuO}_{3-\delta}$ (LCC) in spite of the occurrence of a small amount of second phases of CuO and $\text{La}_{1.85}\text{Ca}_{0.15}\text{CuO}_{3.95}$ according to XRD analysis. Best performance is achieved in LCC cathode with an ASR value of 0.19 Ω cm⁻² at 800°C under open circuit potential conditions and polarization overpotential of 52 mV at a current density of 0.1 A/cm² at 700°C. From the above results, $\text{La}_{0.7}\text{Ca}_{0.3}\text{CuO}_{3-\delta}$ may be the most promising cathode material from the viewpoint of relatively low thermal expansion, and high electrode activity.

Acknowledgements This work has been supported by the Doctor Discipline Fund of Nanjing University of Technology (BSCX200501). Authors gratefully appreciate and acknowledge the reviewer's critical and constructive comments on the manuscript.

References

- R. Chiba, F. Yoshimura, Y. Sakurai, Solid State Ion. **124**, 281 (1999)
- L. Qiu, T. Ichikawa, A. Hirano, N. Imanishi, Y. Takeda, Solid State Ion. **158**, 55 (2003)
- S. Uhlenbruck, F. Tietz, Mater. Sci. Eng. B **107**, 277 (2004)
- K.T. Lee, A. Manthiram, J. Electrochem. Soc. **152**(1), A197 (2005)
- N. Grunbaum, L. Dessemond, J. Fouletier, F. Prado, A. Caneiro, Solid State Ion. **177**, 907 (2006)
- Z. Shao, S.M. Haile, Nature **431**(9), 170 (2004)
- V.V. Srdic, R.P. Omorjan, J. Seydel, Mater. Sci. Eng. B **116**, 119 (2005)
- T.L. Nguyen, T.K.K. Nozaki, T. Honda, A. Negishi, K. Kato, Y. Iimura, J. Electrochem. Soc. **153**(7), A1310 (2006)
- F.S. Baumann, J. Fleig, M. Konuma, U. Starke, H.U. Habermeier, J. Maier, J. Electrochem. Soc. **152**(10), A2074 (2005)
- Z.P. Shao, H. Dong, G.X. Xiong, Y. Cong, W.S. Yang, J. Membr. Sci. **183**, 181 (2001)
- H.C. Yu, K.Z. Fung, J. Power Sources **133**, 162 (2004)

12. H.C. Yu, K.Z. Fung, *Mater. Res. Bull.* **38**, 231 (2003)
13. H.C. Yu, F Zhao, A.V. Virkar, K.Z. Fung, *J. Power Sources* **152**, 22 (2005)
14. M.Z. Zheng, X.M. Liu, W.H. Su, *J. Alloy. Compd.* **395**, 300 (2005)
15. H. Hayashi, M. Kanoh, C.J. Quan, H. Inaba, S.R. Wang, M. Dokuya, H. Tagawa, *Solid State Ion.* **132**, 227 (2000)
16. G. Coffey, J. Hardy, O. Marina, L. Pederson, P. Rieke, E. Thomsen, *Solid State Ion.* **175**, 73 (2004)
17. I. Kaus, H.U. Anderson, *Solid State Ion.* **129**, 189 (2000)
18. S.J. Skinner, C. Munnings, *Mater. Lett.* **57**, 594 (2002)
19. M.A. Daroukh, V.V. Vashook, H. Ullmann, F. Tietz, I. Arual Raj, *Solid State Ion.* **158**, 141 (2003)
20. W.X. Chen, T.L. Wen, H.W. Nie, R. Zheng, *Mater. Res. Bull.* **38**, 1319 (2003)
21. M. Mori, Y. Hiei, N.M. Sammes, G.A. Tompsett, *J. Electrochem. Soc.* **147**, 1295 (2000)
22. S.P. Jiang, J.G. Love, Y. Ramprakash, *J. Power Sources* **110**, 201 (2002)
23. H. Lv, Y. J. Wu, B. Huang, B.Y. Zhao, K.A. Hu, *Solid State Ion.* **177**, 901 (2006)
24. H.S. Song, S.H. Hyun, J. Moon, R.H. Song, *J. Power Sources* **145**, 272 (2005)
25. T. Horita, K. Yamaji, N. Sakai, H. Yokokawa, E. Ivers-Tiffée, *Electrochim. Acta* **46**, 1837 (2001)
26. S. Bebelis, N. Kotsionopoulos, A. Mai, D. Rutenbeck, F. Tietz, *Solid State Ion.* **177**, 1843 (2006)
27. H.R. Rim, S.K. Jeung, E. Jung, J.S. Lee, *Mater. Chem. Phys.* **52**, 54 (1998)
28. K. Murata, T. Fukui, H. Abe, M. Naito, K. Nogi, *J. Power Sources* **145**, 257 (2005)